American Journal of Energy Research, 2024, Vol. 12, No. 1, 1-7
Available online at http://pubs.sciepub.com/ajer/12/1/1
Published by Science and Education Publishing
DOI:10.12691/ajer-12-1-1

Modeling and Analysis of a Mixed Sn-Ge Lead Free Perovskite Based Solar Cells

S. Seck*, A. Sow, M. S. Mané, A. Ndiaye, E. M. Keita, B. Ndiaye, B. Mbow, C. Sène

Physics Department, Faculty of Sciences and Technology, Laboratory of Semiconductors and Solar Energy, University Cheikh Anta Diop, Dakar Country
*Corresponding author: saliouseck1989@gmail.com

Received January 09, 2024; Revised February 10, 2024; Accepted February 16, 2024

Abstract Recently, organic/inorganic hybrid perovskite materials have attracted particular interest in the research community for future generations of photovoltaic systems, due to their manufacturing process ease by solution treatment, their low cost and exceptional optoelectronic properties. Owing mainly to these superior optoelectronic properties and the long carrier lifetime in these materials, perovskite-based photovoltaic devices have achieved high conversion efficiencies up to 25%. However, the presence of lead which is very environmental and human harmful together with the stability issues of these materials constitute major problems encountered in the development of photovoltaic devices based on these materials. Faced with these problems, a large number of alternative absorber materials based on lead-free perovskites and/or inorganic perovskites are increasingly being explored. In this work, we carried out a modeling study of photovoltaic devices using the $CH_3NH_3Sn_{1-y}Ge_yI_3$ lead-free perovskite as absorbing material. The $ZnO(n^+)/Cu_2O(n)/CH_3NH_3Sn_{1-y}Ge_yI_3(p)$ structure is considered for this purpose in which $0 \leqslant y \leqslant 1$. The evolution of the internal quantum efficiency is analyzed as a function of the relative proportion of tin and germanium in the perovskite and also as a function of various other parameters including the thickness of the base and the minority carrier diffusion length in this material. The substitution of lead by metals such as tin and/or germanium leads to lead-free perovskites having opto-electronic properties adapted to the production of high-performance photovoltaic devices. Materials of high optoelectronic and structural properties are in particular obtained for Ge content in the perovskite less than 0.50. In this range of the Ge content, our study shows that the best photovoltaic devices are obtained for values of the germanium (Ge) content close to 0.25

Keywords: *perovskite, photovoltaic cell, quantum efficiency, diffusion length, absorber thickness*

Cite This Article: S. Seck, A. Sow, M. S. Mané, A. Ndiaye, E. M. Keita, B. Ndiaye, B. Mbow, and C. Sène, "Modeling and Analysis of a Mixed Sn-Ge Lead Free Perovskite Based Solar Cells." *American Journal of Energy Research*, vol. 12, no. 1 (2024): 1-7. doi: 10.12691/ajer-12-1-1.

1. Introduction

Organic/inorganic hybrid perovskite materials continue to receive particular attention from the research community for future generations of photovoltaic systems, due to a manufacture ease by solution treatment, a low cost, and exceptional optoelectronic properties [1,2]. Owing mainly to these superior optoelectronic properties and the long carrier lifetime in these materials, perovskite-based photovoltaic devices have achieved high conversion efficiencies up to 25 % [3]. Despite these high performances, the presence of lead which is very harmful to humans and environment represents a major problem. In addition, most lead-based perovskites tend to degrade in the presence of moisture or when exposed to open air. A second major problem arises therefore with regard to the long-term stability and use of solar cells based on lead containing perovskite materials. A large number of alternative absorber materials based on lead-free perovskites and/or inorganic perovskites are increasingly being explored in order to cope with these difficulties.

Among the alternative lead-free materials used, the mixed perovskites based on tin and germanium have been the subject of recent work to improve the stability of the devices while maintaining high photovoltaic performance and environment respect [4,5]. Nagane and al. [6] have synthesized mixed Sn-Ge $CH_3NH_3Sn_{(1-y)}Ge_yI_3$ perovskites in which $0 \leq y \leq 1$. Up to 50% substitution of Ge at the Sn site in $CH_3NH_3SnI_3$, they found that the perovskites remain in a tetragonal phase (P4mm). Above 50% Ge in the perovskite, a transition from tetragonal to trigonal phase was observed [6]. The origin of this phenomenon is said to be due to the large difference in size between metallic ions Sn^{2+} (1.35 Å) and Ge^{2+} (0.73 Å) [6,7,8]. They have shown that these lead-free Sn-Ge mixed perovskites are direct-gap semiconductors with bandwidths ranging from 1.38eV to 2.0 eV, suitable for a wide range of applications, from light-emitting diodes to solar cell manufacturing

Recently, two-dimensional (2D) perovskite materials have also attracted much interest due to their greater water resistance and stability than three-dimensional (3D) perovskites [9]. The structures of these 2D perovskites offer the possibility to adjust their band width and the dynamics of the charge carriers [10]. Moreover, they would have a high optical absorption ($\sim 10^5 cm^{-1}$) throughout the UV-vis region, high photoluminescence values, longer carrier lifetime and could attain a fairly high conversion efficiency of up to 25.76%, which would make them competitive with respect to perovskite-based solar cells reported in the literature [11,12].

Assuming that two-dimensional (2D) perovskites can be experimentally produced, $CH_3NH_3Sn_{(1-y)}Ge_yI_3$, Kar and al. [13] systematically studied their stability and structural properties for $0 \le y \le 0.5$

In the present work we have carried out a modeling study of the internal quantum efficiency of the photovoltaic cell based on lead free perovskite, $CH_3NH_3Sn_{(1-y)}Ge_yI_3$ with $0 \le y \le 1$. For this purpose, the $ZnO(n^+)/Cu_2O(n)/CH_3NH_3Sn_{1-y}Ge_yI_3(p)$ structure have been considered with ZnO and Cu_2O window layers having 3.0 eV and 2.1 eV bandwidth, respectively. Cu_2O, which acts as a buffer layer, also ensures good electrical contact and transition between the absorber and the ZnO layer.

2. $CH_3NH_3Sn_{(1-y)}Ge_yI_3$ Pérovskite Based Photovoltaïc Solar Cell Structure

The solar cell model used in this work is illustrated in Figure 1.

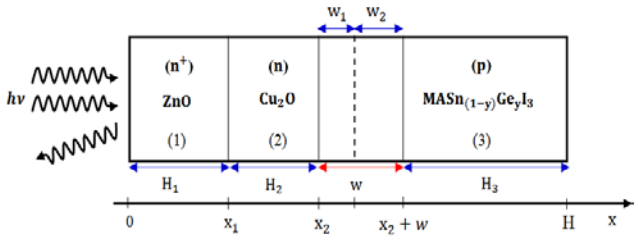

Figure 1. $CH_3NH_3Sn_{(1-y)}Ge_yI_3$ perovskite solar cell Model

Its structure is $n^+ - ZnO / Cu_2O(n) / p - CH_3NH_3Sn_{1-y}Ge_yI_3$.

The absorber layer is the perovskite $CH_3NH_3Sn_{1-y}Ge_yI_3$ material. It is a p-type semiconductor material and has the function of absorbing incident photons from solar radiation to generate electron-hole pairs. The particular feature of this material is to have a forbidden band whose width can be modulated according to the proportion of germanium it contains. The forbidden bandwidth is 1.3 eV for $CH_3NH_3SnI_3$ (y = 0) and 2.0 eV for $CH_3NH_3SnI_3$ (y = 1). Thus, by varying the germanium content, we can also continuously vary the band gap width between 1.3 eV and 2.0 eV and make different solar cells.

The thin n-type Cu_2O copper oxide layer called buffer layer, of about 50 nm thick is deposited on the $CH_3NH_3Sn_{1-y}Ge_yI_3$ surface. This n-type semiconductor layer provides the n-p junction with the absorber and acts as an interface with the window layer. With a direct gap width of 2.1 eV and its non-toxicity, Cu_2O is considered to be one of the most promising materials for photovoltaic applications.

The zinc oxide (ZnO) window layer, which is a transparent conductive oxide (TCO), completes the structure of the solar cell. It consists of two layers. First a thin intrinsic ZnO layer of about 50 nm thick is used to cover the buffer layer and also to reduce short circuits. The window layer is then supplemented by an aluminum-doped ZnO layer (ZnO: Al) deposition, with a thickness in the range of 0.5 µm to 1 µm. The highly Al-doped ZnO layer has a high conductivity and is very transparent. It allows the incident photons to pass to the absorber layer and also allows a good collection of charge carriers due to its high conductivity.

3. Theoretical Approach and Model

The equations used to model the solar cell operation are based on the minority carrier continuity equations in each part of the solar cell. These continuity equations make it possible to study all the phenomena that occur in semiconductors and to determine the properties of the devices manufactured using these materials.

It is assumed in the following parts that the space charge zone is located between the n-type Cu_2O and the p-type $CH_3NH_3Sn_{1-y}Ge_yI_3$. The electric field is also assumed to be zero outside this region. In the case of steady-state conditions, the continuity equations are given by:

$$\frac{1}{q} div\overrightarrow{J_n} + G_n - R_n = 0 \quad (1)$$

$$-\frac{1}{q} div\overrightarrow{J_p} + G_p - R_p = 0 \quad (2)$$

In the absence of an electric field, we can write:

$$\overrightarrow{J_n} = qD_n . \overrightarrow{grad}(n) \quad (3)$$

$$\overrightarrow{J_p} = -qD_p . \overrightarrow{grad}(p) \quad (4)$$

Our calculations are limited to the one-dimensional case.

Figure 2 and figure 3 show the variations of the ZnO and Cu_2O absorption coefficients and the variations of the $CH_3NH_3Sn_{1-y}Ge_yI_3$ absorption coefficients with photon energy, respectively. All absorption coefficient values are obtained from the literature [6,14,15].

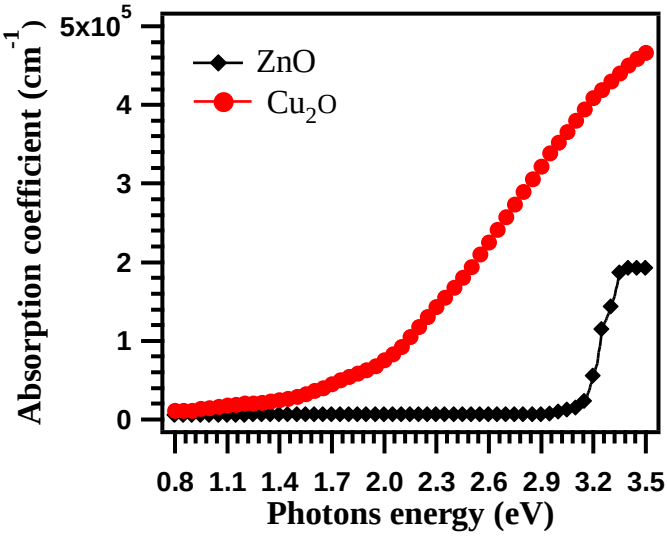

Figure 2. Absorption coefficient of ZnO and Cu_2O layers [14,15]

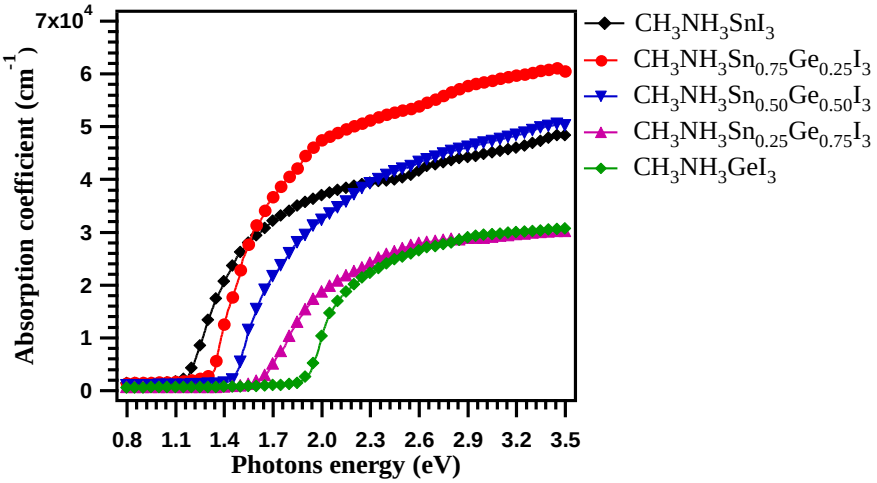

Figure 3. Absorption coefficient of $CH_3NH_3Sn_{(1-y)}Ge_yI_3$ layers [6]

3.1. Current Density Generated By Light in the Emitter

The current density $J_{ph,E}$ generated by incident photons in the emitter comprises two contributions: the current density generated in the n^+-ZnO region, J_{ph_1} and the current density generated in the $n-Cu_2O$ region J_{ph_2}

$$J_{ph,E} = J_{ph_1} + J_{ph_2} \quad (5)$$

3.1.1. Current Density Generated in the n^+ Region

In the ZnO window layer where minority carriers are the holes, the continuity equation is given by:

$$\frac{d^2\Delta_{p_1}}{dx^2} - \frac{\Delta_{p_1}}{{L_{p_1}}^2} = -\frac{g_{ZnO}}{D_{p_1}} \quad (6)$$

Where:

$g_{ZnO} = \alpha_{ZnO} F(1-R) e^{-\alpha_{ZnO} x}$ and ${L_{p_1}}^2 = D_{p_1}\tau_{p_1}$

In this equation Δ_{p_1} is the minority carrier concentration, L_{p_1} and D_{p_1} are the hole diffusion length and the hole diffusion coefficient in the ZnO region, respectively.

τ_{p_1} and α_{ZnO} represent the hole lifetime and absorption coefficient of the ZnO window layer, respectively.

R is the reflection coefficient and $F(E,\lambda)$ is incident photon flux of energy E and wavelength $\lambda(\mu m)$.

The resolution of this equation was made taking into account the following boundary conditions:

$$D_{p_1}\frac{\partial\Delta_{p_1}}{\partial x} = S_{p_1}\times\Delta_{p_1} \rightarrow \text{for } x = 0 \quad (7)$$

$$\Delta_{p_1} = 0 \rightarrow \text{for } x = x_1 \quad (8)$$

Where S_{p_1} is the recombination velocity on the front surface of the window layer.

The photocurrent J_{ph_1} in this region is given by:

$$J_{ph_1} = -qD_{p_1}\frac{\partial\Delta_{p_1}(x_1)}{\partial x} \quad (9)$$

$$J_{ph_1} = \frac{q\alpha_{ZnO}F(1-R)L_{p_1}}{(\alpha_{ZnO}{}^2L_{p_1}{}^2-1)}\left\{\frac{\left(\frac{S_{p_1}L_{p_1}}{D_{p_1}}+\alpha_{ZnO}L_{p_1}\right)-e^{-\alpha_{ZnO}x_1}\left[\frac{S_{p_1}L_{p_1}}{D_{p_1}}ch\left(\frac{x_1}{L_{p_1}}\right)+sh\left(\frac{x_1}{L_{p_1}}\right)\right]}{\frac{S_{p_1}L_{p_1}}{D_{p_1}}sh\left(\frac{x_1}{L_{p_1}}\right)+ch\left(\frac{x_1}{L_{p_1}}\right)}-\alpha_{ZnO}L_{p_1}e^{-\alpha_{ZnO}x_1}\right\} \quad (10)$$

3.1.2. Current Density Generated in Region n

In the buffer layer which consists in a thin n-type Cu_2O layer, minority carriers also the holes. The continuity equation for the minority carriers in this copper oxide layer is given by:

$$\frac{d^2\Delta_{p2}}{dx^2}-\frac{\Delta_{p2}}{L_{p_2}{}^2}=-\frac{g_{Cu_2O}}{D_{p2}} \quad (11)$$

Where $g_{Cu_2O}=\alpha_{Cu_2O}F(1-R)e^{-\alpha_{ZnO}x_1}.e^{-\alpha_{Cu_2O}(x-x_1)}$ and $L_{p_2}{}^2=D_{p2}\tau_{p2}$

L_{p2} and D_{p2} are the hole diffusion length and in the hole diffusion coefficient in copper oxide layer, respectively.

τ_{p2} and α_{Cu_2O} are the hole lifetime and the absorption coefficient in the Cu_2O buffer layer, respectively.

Taking into account the following boundary conditions defined as follows,

$$D_{p2}\frac{\partial\Delta_{p2}}{\partial x}=S_{p2}\times\Delta_{p2}+D_{p1}\times\frac{\partial\Delta_{p1}}{\partial x}\rightarrow \text{for } x=x_1 \quad (12)$$

$$\Delta_{p2}=0\rightarrow \text{for } x=x_2 \quad (13)$$

the photo-current in the region $x_1\le x\le x_2$ is given by :

$$J_{ph2}=-qD_{p2}\frac{\partial\Delta_{p2}(x_2)}{\partial x} \quad (14)$$

$$J_{ph_2}=\frac{q\alpha_{Cu_2O}F(1-R)L_{p_2}e^{-\alpha_{ZnO}x_1}}{\left(\alpha_2{}^2L_{p_2}{}^2-1\right)}\left\{\frac{\left(\frac{S_{p_2}L_{p_2}}{D_{p_2}}+\alpha_{Cu_2O}L_{p_2}\right)-e^{-\alpha_{Cu_2O}(x_2-x_1)}\left[\frac{S_{p_2}L_{p_2}}{D_{p_2}}ch\left(\frac{x_2-x_1}{L_{p_2}}\right)+sh\left(\frac{x_2-x_1}{L_{p_2}}\right)\right]}{\frac{S_{p_2}L_{p_2}}{D_{p_2}}sh\left(\frac{x_2-x_1}{L_{p_2}}\right)+ch\left(\frac{x_2-x_1}{L_{p_2}}\right)}-\alpha_{Cu_2O}L_{p_2}e^{-\alpha_{Cu_2O}(x_2-x_1)}\right\}+\frac{J_{p_1}(x_1)}{\frac{S_{p_2}L_{p_2}}{D_{p_2}}sh\left(\frac{x_2-x_1}{L_{p_2}}\right)+ch\left(\frac{x_2-x_1}{L_{p_2}}\right)} \quad (15)$$

3.2. Current Density Generated in the Space Charge Area

In this region, charge carrier recombination may be neglected. Indeed, it is assumed that the transit time of the free carriers in this zone is much shorter than their lowest lifetime because of the strong electric field which prevails therein. So, carriers will not have time to recombine and will all be collected.

In the space charge region, the current expression is given by:

$$J_{ZCE}=-qF(1-R)e^{-\alpha_{ZnO}x_1}e^{-\alpha_{Cu_2O}(x_2-x_1)}\left[e^{-\alpha_{Cu_2O}w_1}-1\right]-qF(1-R)e^{-\alpha_{ZnO}x_1}e^{-\alpha_{Cu_2O}\left[(x_2+w_1)-x_1\right]}\left[e^{-\alpha_{MASGI}w_2}-1\right] \quad (16)$$

3.3. Current Density Generated in the P Region

In this absorber layer, the photocurrent is an electron due current. The continuity equation of minority carriers (electrons) is given by:

$$\frac{d^2\Delta_{n3}}{dx^2}-\frac{\Delta_{n3}}{L_{n_3}{}^2}=-\frac{g_{MASGI}}{D_{n_3}} \quad (17)$$

Where:

$g_{MASGI}=\alpha_{MASGI}F(1-R)e^{-\alpha_{ZnO}x_1}.e^{-\alpha_{Cu_2O}\left[(x_2+w_1)-x_1\right]}.e^{-\alpha_{MASGI}\left[x-(x_2+w_1)\right]}$ and

$L_{n_3}{}^2=D_{n_3}\tau_{n_3}$

Δ_{n3} and L_{n_3} are the electron concentration and the electron diffusion length in the p region, respectively.

D_{n_3} and τ_{n_3} are electron diffusion coefficient and electron lifetime in the p region, respectively.

α_{MASGI} is the absorption coefficient of the $CH_3NH_3Sn_{(1-x)}Ge_xI_3$ layer

With boundary conditions defined as follows:

$$D_{n_3}\frac{\partial\Delta_{n3}}{\partial x}=-S_{n_3}\times\Delta_{n3}\rightarrow \text{for } x=H \quad (18)$$

$$\Delta_{n_3}=0\rightarrow \text{for } x=x_2+w \quad (19)$$

we get the following expression for the photocurrent in the absorber layer:

$$J_{ph3}=qD_{n3}\frac{\partial\Delta_{n3}(x_2+w)}{\partial x} \quad (20)$$

$$J_{ph_3}=-\frac{q\alpha_{MASGI}F(1-R)L_{n_3}e^{-\alpha_{ZnO}x_1}e^{-\alpha_{Cu_2O}(x_2-x_1+w_1)}}{(\alpha_2{}^2L_{n_3}{}^2-1)}\times\left\{\frac{\left(\alpha_{MASGI}L_{n_3}-\frac{S_{n_3}L_{n_3}}{D_{n_3}}\right)e^{-\alpha_{MASGI}[H-(x_2+w_1)]}+e^{-\alpha_{MASGI}w_2}\left[\frac{S_{n_3}L_{n_3}}{D_{n_3}}ch\left(\frac{H-(x_2+w)}{L_{n_3}}\right)+sh\left(\frac{H-(x_2+w)}{L_{n_3}}\right)\right]}{\frac{S_{n_3}L_{n_3}}{D_{n_3}}sh\left(\frac{H-(x_2+w)}{L_{n_3}}\right)+ch\left(\frac{H-(x_2+w)}{L_{n_3}}\right)}-\alpha_{MASGI}L_{n_3}e^{-\alpha_{MASGI}w_2}\right\} \quad (21)$$

3.4. Expression of the Total Photocurrent

The total photocurrent results from the contributions of the different parts of the cell. For a given wavelength, it represents the sum of all the above calculated current components that include the hole diffusion current in the ZnO and Cu_2O regions, the current generated in the space charge zone, and the electron diffusion current in the p-type region.

$$J_{Ph,T}=J_{ph,E}+J_{ZCE}+J_{ph3} \quad (22)$$

The internal quantum efficiency is then given:

$$IQE = \frac{J_{Ph,T}}{qF(1-R)} \quad (23)$$

4. Results and Discussion

In this section our investigations are focused on the effects of the germanium (Ge) content in the absorber layer and on some geometric parameters on the internal quantum efficiency of the $ZnO(n^+)/Cu_2O(n)/CH_3NH_3Sn_{1-y}Ge_yI_3(p)$ structure which theoretically models our lead-free perovskite based solar cell.

4.1. Internal quantum efficiency

Internal quantum efficiency is a characterization tool used to determine the effect of device parameters during the fabrication step but also during the development and production of solar cells. Knowing the impact of these parameters makes it possible to predict the characteristics of the cell having the best performance. The evolution of the internal quantum efficiency of our solar cell as function of photon energy is shown in Figure 4 for various values of the germanium (Ge) content in the $CH_3NH_3Sn_{1-y}Ge_yI_3$ perovskite material. The carrier diffusion lengths in regions 1 and 2 are set to 0.55 µm and 0.5 µm, respectively, with thicknesses of 0.55 µm and 0.05 µm. The thickness of the absorber $CH_3NH_3Sn_{1-y}Ge_yI_3$ is set at 0,5 µm and the diffusion length of the carriers is estimated at 0,5 µm.

A shift toward higher energies is observed in the absorption onset when increasing the germanium (Ge) content in the absorber material, in good accordance with the change in the band gap width when varying this parameter. In the low photon energy range, the internal quantum efficiency is very low and increases very slightly with photon energy for each value of the germanium (Ge) content in the absorber layer. For photon energies above the absorption edge, the internal quantum efficiency increases sharply with energy up to a maximum value depending on the germanium (Ge) content in the layer. Within this range of photon energies, one can note that the quantum efficiency does not change monotonically with the germanium (Ge) content in the absorbent layer. For germanium (Ge) content values considered in this work $(0 \le y \le 1)$ and for a step variation of 0.25, an increase in the maximum quantum efficiency is first observed from 62.9% for y = 0 $(E_g = 1.30eV)$ to 65.8% corresponding to y = 0.25 $(E_g = 1.43eV)$. Beyond y = 0.25, the maximum quantum efficiency decreases more rapidly passing through 60.7% for y = 0.50 $(E_g = 1.67eV)$, 53.9% for y = 0.75 $(E_g = 1.76eV)$ and 52.2% for y = 1 $(E_g = 2.00eV)$.

It is well known that solar cell performances depend mainly on the absorption of light by the absorbing layer and they become very important when the junction is well suited to the solar spectrum. From the technological point of view, the absorber layer must have an optimal gap to absorb the widest range of wavelengths of the solar spectrum with a high absorption coefficient. The theoretical optimum of the optical gap of an absorber material in a solar cell is estimated to be about 1.40 eV. This could explain the largest 65.8% response obtained for y = 0.25 corresponding to the perovskite $CH_3NH_3Sn_{0,75}Ge_{0,25}I_3$ (Eg = 1.43 eV).

In the range values $0 \le y \le 0.25$ of the Ge content in the material, Nagane and al. [6] have shown that the perovskite is in the tetragonal phase. For Ge content in the perovskite greater than or equal to 50%, the band gap width is larger than the theoretical optimum and these authors highlighted the occurrence of a transition from the tetragonal phase to the trigonal phase, which would be due to the large difference in size between Sn^{2+} (atomic radius 1.35 Å) [7] and Ge^{2+} (atomic radius 0.73 Å) [8] and which makes the perovskite unstable and degrades the solar cell performances.

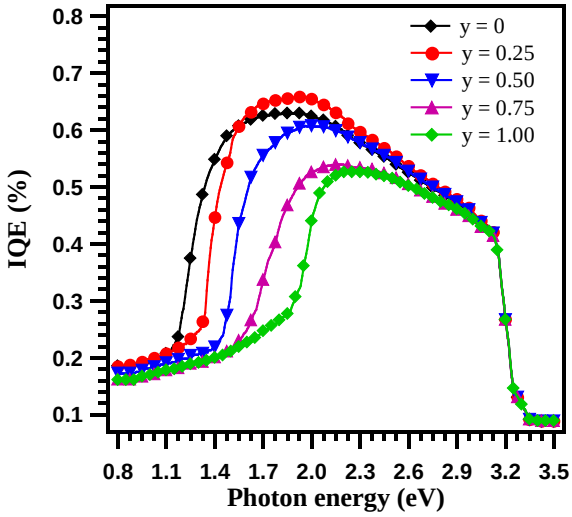

Figure 4. Internal quantum efficiency vs photon energy for various values of Ge $(0 \le y \le 1)$ Content in the $ZnO(n^+)/Cu_2O(n)/CH_3NH_3Sn_{1-y}Ge_yI_3(p)$ solar cell

The highest internal quantum efficiency in this experience is obtained for a value of y = 0.25, corresponding to $CH_3NH_3Sn_{0,75}Ge_{0,25}I_3$. This can also be explained by the fact that $CH_3NH_3Sn_{0,75}Ge_{0,25}I_3$ has absorption coefficients higher than those of $CH_3NH_3SnI_3$, $CH_3NH_3Sn_{0,5}Ge_{0,5}I_3$, $CH_3NH_3Sn_{0,25}Ge_{0,75}I_3$, and $CH_3NH_3GeI_3$, as illustrated in Figure 3, which represents the absorption coefficients as functions of germanium (Ge) content values in the $CH_3NH_3Sn_{1-y}Ge_yI_3$ perovskite. These absorption coefficients were given by Nagane and al. [6] and completed by us for energy photons ranging from 0.8 eV to 3.5 eV. From this study, the best internal quantum efficiency is expected for low Ge contents (y close to 0.25) in the lead-free perovskite material.

4.1.1. Influence of the Diffusion Length of Minority Carriers in the Absorber

The minority carrier diffusion length is an important parameter for semiconductor-based devices operation. It is linked to carriers' lifetime and diffusion coefficients, which depend very much on the material's physico-chemical properties. The internal quantum efficiency of the $ZnO\left(n^{+}\right)/Cu_2O(n)/CH_3NH_3Sn_{0,75}Ge_{0,25}I_3$ solar cell is depicted in figure 5 as functions of the photon energy for different values of the electron diffusion length in the absorber layer $CH_3NH_3Sn_{0.75}Ge_{0.25}I_3$. The diffusion lengths of the holes in regions 1 and 2 are 0.55 µm and 0.5 µm, respectively, with thicknesses of 0.55 µm and 0.05 µm. The thickness of $CH_3NH_3Sn_{0,75}Ge_{0,25}I_3$ is set at 0.5 µm and the diffusion length ranges from 0.1 µm to 0.7 µm.

In the energy range between 1.30 eV and 3.00 eV, the internal quantum efficiency increases with the minority carrier diffusion length up to a maximum value of 68%. In this energy range, photons reach the base and are absorbed, producing electron-hole pairs that diffuse into the cell to contribute to the current. Beyond the energies of 2.00 eV, the internal quantum efficiency decreases. This decrease in efficiency is due to photon absorption by Cu_2O and ZnO layers in regions 1 and 2 of the solar cell, respectively.

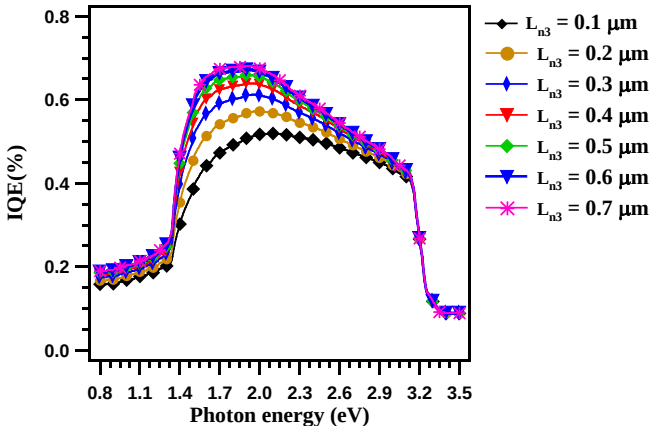

Figure 5. Influence of absorber scattering length on spectral response for y = 0.25

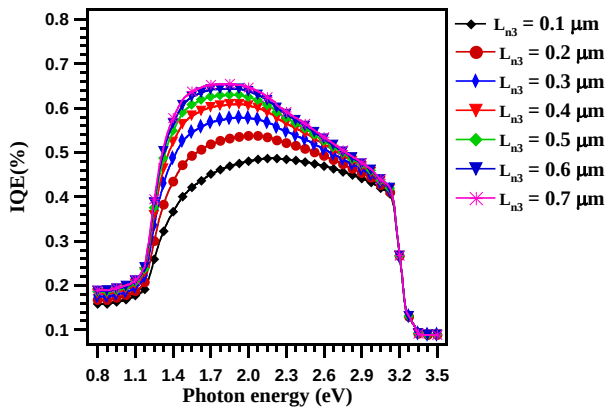

Figure 6. Influence of the absorber minority carrier diffusion length on the internal quantum efficiency of the solar cell for y = 0

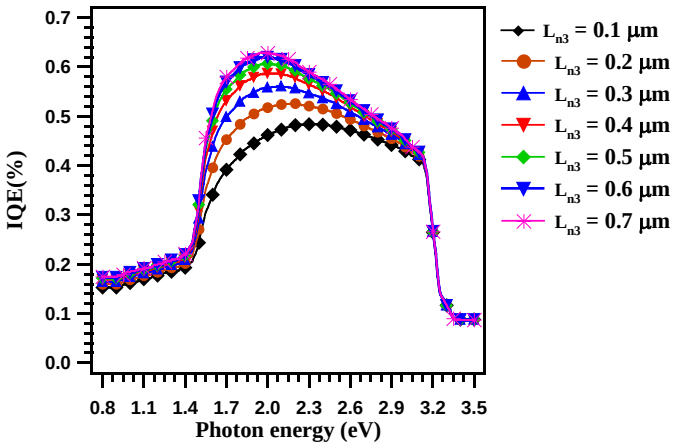

Figure 7. Influence of the absorber minority carrier diffusion length on the internal quantum efficiency of the solar cell for y = 0.50

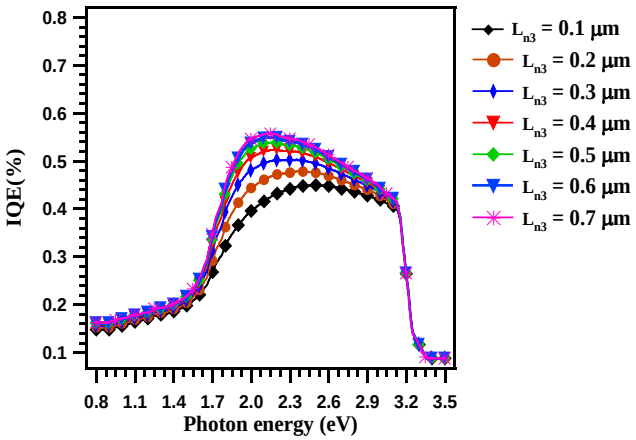

Figure 8. Influence of the absorber minority carrier diffusion length on the internal quantum efficiency of the solar cell for y = 0.75

Figures 6, 7 and 8 illustrate the internal quantum efficiency of the $CH_3NH_3Sn_{1-y}Ge_yI_3$ alloy for y = 0, y = 0.50 and y = 0.75 as functions of the energy for different values of diffusion length. For these different values of y, a similar shape as for y = 0.25 is observed for the internal quantum efficiency, with lower maximum responses that move to higher energies compared to the case of y = 0.25. The maximum internal quantum efficiency is 65.4% (y = 0), 63% (y = 0.5), 55.7% (y = 0.75).

4.1.2. Influence of the Absorber Thickness on the Internal Quantum Efficiency

Figure 9 shows the influence of the thickness of the $CH_3NH_3Sn_{0.75}Ge_{0.25}I_3$ absorber layer on the internal quantum efficiency of the solar cell. The diffusion length of the base is fixed at 0.5 µm. The diffusion lengths of the holes in regions 1 and 2 are 0.55 µm and 0.5 µm, respectively, with thicknesses of 0.55 µm and 0.05 µm. The thickness of the absorber layer ranges from 0.1 µm to 0.7 µm. For low thickness values, internal quantum efficiency remains low at 53.4%. The maximum internal quantum efficiency of 65.8% is obtained with a thickness value of 0.5 µm. Beyond this value, the spectral response remains almost constant.

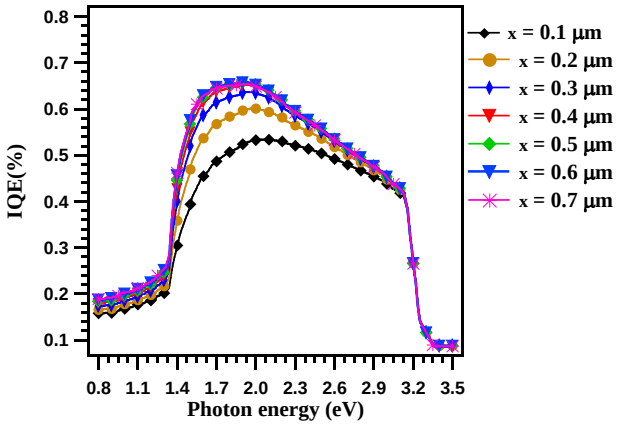

Figure 9. Influence of the absorbent layer thickness on the internal quantum efficiency

5. Conclusion

In this work a modeling study of photovoltaic devices using lead-free $CH_3NH_3Sn_{(1-y)}Ge_yI_3$ perovskites as absorber material has been carried out. The photovoltaic cell is structured as $ZnO(n^+)/Cu_2O(n)/CH_3NH_3Sn_{1-y}Ge_yI_3(p)$. The partial substitution of tin by germanium $CH_3NH_3SnI_3$ results in $CH_3NH_3Sn_{(1-y)}Ge_yI_3$ with a widening of the forbidden band width of the perovskite and in modifications of its crystallographic structure. The internal quantum efficiency of the $CH_3NH_3Sn_{(1-y)}Ge_yI_3$ based photovoltaic cell has been analyzed as function of the germanium (Ge) content in the absorber material and by varying some geometrical and electrical parameters (base thickness and minority carrier diffusion length). Our study shows that this substitution has a beneficial effect on the internal quantum efficiency of the solar cell only for low germanium (Ge) contents in the perovskite. The best internal quantum efficiency is expected for values of the germanium (Ge) contents in the lead-free perovskite absorber material close to 0.25 and for an absorber thickness of about 0.5 µm.

References

[1] H. Tsai, W. Nie, J. C. Blancon, C. C. Stoumpos, R. Asadpour, B. Harutyunyan, A. J. Neukirch, R. Verduzco, J. J. Crochet, S. Tretiak, et al., High-efficiency twodimensional Ruddlesden-Popper perovskite solar cells, Nature, 536 (2016) 312−316.

[2] D. Ghosh, A. J. Neukirch, S. Tretiak, Optoelectronic properties of two-dimensional bromide perovskites: Influences of spacer cations, J. Phys. Chem. Lett., 11 (2020) 2955−2964.

[3] National renewable energy laboratory (NREL). Best research-cell efficiencies. https://www.nrel.gov/pv/assets/images/efficiency-chart.png.

[4] M. G. Ju, J. Dai, L. Ma, X. C. Zeng, Lead-free mixed tin and germanium perovskites for photovoltaic application, J. Am. Chem. Soc., 139 (2017) 8038−8043.

[5] P. Cheng, T. Wu, J. Liu, W. Q. Deng, K. Han, Lead-free, two-dimensional mixed germanium and tin perovskites, J. Phys. Chem. Lett., 9 (2018) 2518−2522.

[6] S. Nagane, D. Ghosh, R. L. Z. Hoye, B. Zhao, S. Ahmad, A. B. Walker, M. S. Islam, S. Ogale, A. Sadhanala, Lead-free perovskite semiconductors based on germanium-tin solid solutions: Structural and optoelectronic properties, J. Phys. Chem. C, 122 (2018) 5940−5947.

[7] Z. Shi, J. Guo, Y. Chen, Q. Li, Y. Pan, H. Zhang, Y. Xia, W. Huang, Lead-free organic-inorganic hybrid perovskites for photovoltaic applications: Recent advances and perspectives, Adv. Mater, 29 (2017) 1605005.

[8] R. D. Shannon, Revised effective ionic radii and systematic studies of interatomic distances in halides and chalcogenides, Acta Crystallogr., Sect. A: Cryst. Phys., Diffr., Theor. Gen. Crystallogr., 32 (1976) 751−767.

[9] E. Shi, Y. Gao, B. P. Finkenauer, A. Akriti, A. H. Coffey, L. Dou, Two-dimensional halide perovskite nanomaterials and heterostructures, Chem. Soc. Rev., 47 (2018) 6046−6072.

[10] V. D'Innocenzo, A. R. Srimath Kandada, M. De Bastiani, M. Gandini, A. Petrozza, Tuning the light emission properties by band gap engineering in hybrid lead halide perovskite, J. Am. Chem. Soc., 136 (2014) 17730-17733.

[11] L. Dou, A. B. Wong, Y. Yu, M. Lai, N. Kornienko, S. W. Eaton, A. Fu, C. G. Bischak, J. Ma, T. Ding, et al., Atomically thin twodimensional organic-inorganic hybrid perovskites, Science, 349 (2015) 1518-1521.

[12] L. Zhang, W. Liang, How the structures and properties of twodimensional layered perovskites MAPbI3 and CsPbI3 vary with the number of layers, J. Phys. Chem. Lett., 8 (2017) 1517-1523.

[13] M. Kar, R. Sarkar, S. Pal, P. Sarkar, Lead Free Two-Dimensional Mixed Tin and Germanium Halide Perovskites for Photovoltaic Applications, J. Phys. Chem., 125 (2021) 74−81.

[14] C. Guillén, J. Herrero, Single-phase Cu2O and CuO thin films obtained by low-temperature oxidation processes, Journal of Alloys and Compounds, 17 (2018).

[15] M. R. Islam, M. G. Azam, Enhanced photocatalytic activity of Mg-doped ZnO thin films prepared by sol–gel method, Surface Engineering, (2020).